

Alternating diatomaceous and volcanoclastic deposits in Milos Island, Greece. A contribution to the upper Pliocene–lower Pleistocene stratigraphy of the Aegean Sea

José P. Calvo ^{a,*}, Maria V. Triantaphyllou ^b, Manuel Regueiro ^c, Michael G. Stamatakis ^b

^a *Department of Petrology and Geochemistry, Universidad Complutense de Madrid, Jose Antonio Novais 2, 28040 Madrid, Spain*

^b *Faculty of Geology and Geoenvironment, National and Kapodistrian University of Athens, Panepistimiopolis, 15784 Athens, Greece*

^c *Instituto Geológico y Minero de España, Ríos Rosas 23, 28003 Madrid, Spain*

In the northern part of Milos Island, South Aegean Volcanic Arc, a stratigraphic succession spanning the late Pliocene and early Pleistocene exceeds 300 m in thickness and records an alternation of products from sub-marine volcanic explosive events and fossiliferous, both siliceous and carbonate marine sedimentary rocks. The accumulation of volcanoclastic deposits took place under subaqueous marine conditions as evidenced by sedimentary features, scarce fossil remains and the local presence of burrow traces.

Each major volcanic event was represented by the accumulation of thick-bedded pumice and glassy tuffs, succeeded by the deposition of marine sediments composed mainly of laminated diatomaceous marlstone and sandy limestone. The silica content of the diatomaceous sediments varies from 39% to 70%, mostly in the form of biogenic opal-A. SiO₂/Al₂O₃ ratios ranging from 5 to 21 indicate a varied contribution of reworked volcanic grains. The sequential arrangement of basinal diatomaceous marlstone and shoreface sandy lime-stone deposits suggests that the depth of water was not great, which is also consistent with features observed in the volcanoclastic deposits.

Calcareous nannofossils from the upper part of the succession of northern Milos allow biostratigraphic correlation with nannofossil biozones MNN19a–MNN19b across the Gelasian/Calabrian boundary within the early Pleistocene. A late Pliocene (Piacenzian) age has been estimated for the lower part of the section, where biozone MNN16a has been documented. Diatoms, planktonic foraminifera and calcareous nannofossil assemblages in the diatomaceous beds point to deposition in a partially closed, relatively shallow marine environment. In this setting, warm and stratified water conditions can be concluded for the Piacenzian diatomaceous beds whereas highly productive cool waters are inferred from the Gelasian/Calabrian diatomite.

Keywords: Diatomaceous marlstone; Volcanoclastic rocks; Calcareous nannofossils; Quaternary; South Aegean Volcanic Arc (SAVA)

1. Introduction

The island of Milos is located in the active South Aegean Volcanic Arc (SAVA) (Fig. 1). The SAVA is punctuated by several islands where extensional and subduction-related tectonics as well as a complex history of volcanic episodes throughout the Pliocene and Quaternary is recorded (Angelier et al., 1982; Jackson, 1994; Fytikas and Vougioukalakis, 2005). In Milos Island, volcanic activity started during the late Pliocene (Fytikas et al., 1976; Stewart and McPhie, 2003b, 2006) and is currently represented by high heat flow, thermal springs and the presence of hot soils in the SE part of the island (Fytikas, 1977; Fytikas et al., 1986).

Comprehensive information on the recent geological evolution of Milos was first furnished by Fytikas et al. (1976). However, the time-stratigraphic framework of Milos had remained relatively poorly

established until recent work by Rinaldi and Campos Venuti (2003), who studied the volcanoclastic facies related to the eruption of the Bombarda volcano in the northern part of the island in detail, and by Stewart and McPhie (2003a, 2004). The latter authors provided a stratigraphic framework for the Neogene formations cropping out in the north-eastern sector of the island and proposed an interpretation of some specific volcanic features, e.g. dacite cryptodomes and coarse pumice breccias, included in the Neogene section. Later on, Stewart and McPhie (2006) published an overview of the upper Pliocene and Pleistocene felsic volcanic architecture of Milos Island, reflecting contrasts in eruption style, proximity to source, depositional environment and emplacement processes.

In this paper, a stratigraphic and sedimentological study of the lithological succession cropping out in the area of Alimia–Sarakiniko, northern Milos Island (Figs. 1 and 2), is presented. The stratigraphic succession, which covers the upper Pliocene and lower Pleistocene, can be studied in coastal cliffs and adjacent inland areas starting near Mandrakia and ending about 1 km east of Sarakiniko (Fig. 2).

Diatomaceous marlstone constitutes a dominant facies throughout the succession. Except for the biostratigraphic work by Frydas (1992,

* Corresponding author. Tel.: +34913944902; fax: +34915442535.

E-mail addresses: jpcalvo@geo.ucm.es (J.P. Calvo), mtriant@geol.uoa.gr (M.V. Triantaphyllou), m.regueiro@igme.es (M. Regueiro), stamatakis@geol.uoa.gr (M.G. Stamatakis).

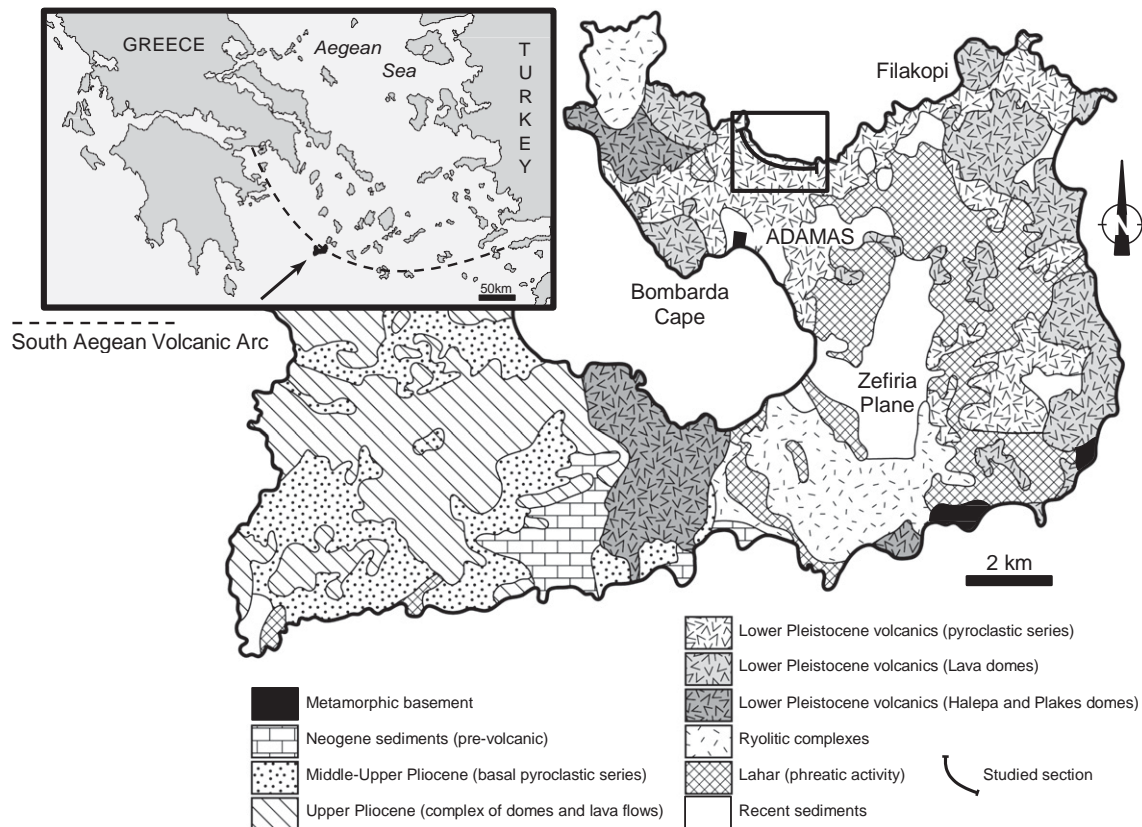


Fig. 1. Geological map of Milos Island (after Fytikas et al., 1986) situated in the west-central part of the South Aegean Volcanic Arc (SAVA) (rectangle). The study area (boxed) is located on the northern part of the island.

1996a, 1996b) and Bellas and Frydas (1994), the presence of diatomaceous deposits in the Plio-Pleistocene stratigraphic record of Milos Island has been poorly documented. Stamatakis et al. (1996, 2010) and Stamatakis (2003) underlined the occurrence of these deposits but did not provide details about stratigraphic and/or sedimentological features. Analysis of the sedimentological, mineralogical, and geochemical features of the diatomaceous marlstone and associated sedimentary rocks provides valuable insight into the complex evolutionary geological framework of northern Milos for the late Pliocene and early Pleistocene. Moreover, micropalaeontological analysis of this facies contributes to its biostratigraphic assignment on the basis of the calcareous nannofossil assemblages.

2. Geological setting

Milos belongs to the Cyclades, a group of islands forming part of the South Aegean Volcanic Arc (Fig. 1). This volcanic chain consists of widely spaced centres in which volcanism is predominantly high-K calc-alkaline (Le Pichon and Angelier, 1979; Zeilunga de Boer, 1989; Francalanci et al., 2007). There is general agreement that the development of the volcanic arc took place throughout the Pliocene and Quaternary as a result of the relative motion of the African and the Aegean plates that gave place to the Hellenic subduction zone (McKenzie, 1978; Le Pichon and Angelier, 1979; Angelier et al., 1982; Meulenkamp et al., 1988; Pe-Piper and Piper, 1989, 2005; Royden and Papanikolaou, 2011).

The geology of Milos was first described by Sonder (1924) and then studied in detail by Fytikas et al. (1976), (1986), Fytikas (1977), and Fytikas and Vougioukalakis (1995). The oldest rocks cropping out in Milos consist of basement metamorphic rocks including mainly schist, gneiss and quartzite of Mesozoic to Palaeogene ages (Fytikas et al., 1976; Fytikas, 1977). The metamorphic basement is overlain

unconformably by upper Miocene to lower Pliocene conglomeratic and calcareous rocks (Fig. 1). Prior to the onset of volcanism, subsidence related to extension of the Aegean lithosphere took place during the early Pliocene, between 5.0 and 4.4 Ma (van Hinsbergen et al., 2004).

From the late Pliocene (~3.0 Ma), the island of Milos has been affected by extensive calc-alkaline volcanism, leading to a complex arrangement of volcanic and volcano-sedimentary deposits of various ages (Fytikas et al., 1986). The volcanic rocks of Milos are mainly rhyolite and dacite with subordinate andesite and basaltic andesite. Fytikas (1977) and Fytikas and Vougioukalakis (1995) distinguished the basal pyroclastic series composed of mainly felsic, pumice-rich flows, tuffs and tuffites with interbedded sedimentary rocks containing marine fauna. This lower volcano-sedimentary succession was succeeded by domes and lava flows of rhyolitic to andesitic composition, accompanied by ejection of pyroclastic materials and ignimbrites. Huge lahar deposits ("Green lahar" of Fytikas, 1977) accumulated later in the western part of Milos. More recent periods of strong volcanic activity are recorded by rhyolite to rhyodacite lavas, pumice and cinders. Fytikas et al. (1976) dated these younger volcanic events at 0.48 Ma, which represents the time of the most recent eruptive phase in Milos and surrounding islets. Additional dating of the volcanic succession in Milos was provided by Fytikas et al. (1986), Traineau and Dalabakis (1989), Kondopoulou and Pavlides (1990), and Stewart and McPhie (2003a, 2003b, 2004). Recently, Rinaldi and Campos Venuti (2003) and Stewart and McPhie (2006) summarised the radiometric ages available from the volcanic units in the northern part of Milos.

The tectonic structure of the island is characterised by a rather dense network of normal faults oriented approximately N-S, E-W and SW-NE. Lava domes and craters are essentially distributed according to this main fault framework (Fytikas et al., 1986; Fytikas and Vougioukalakis, 1995).

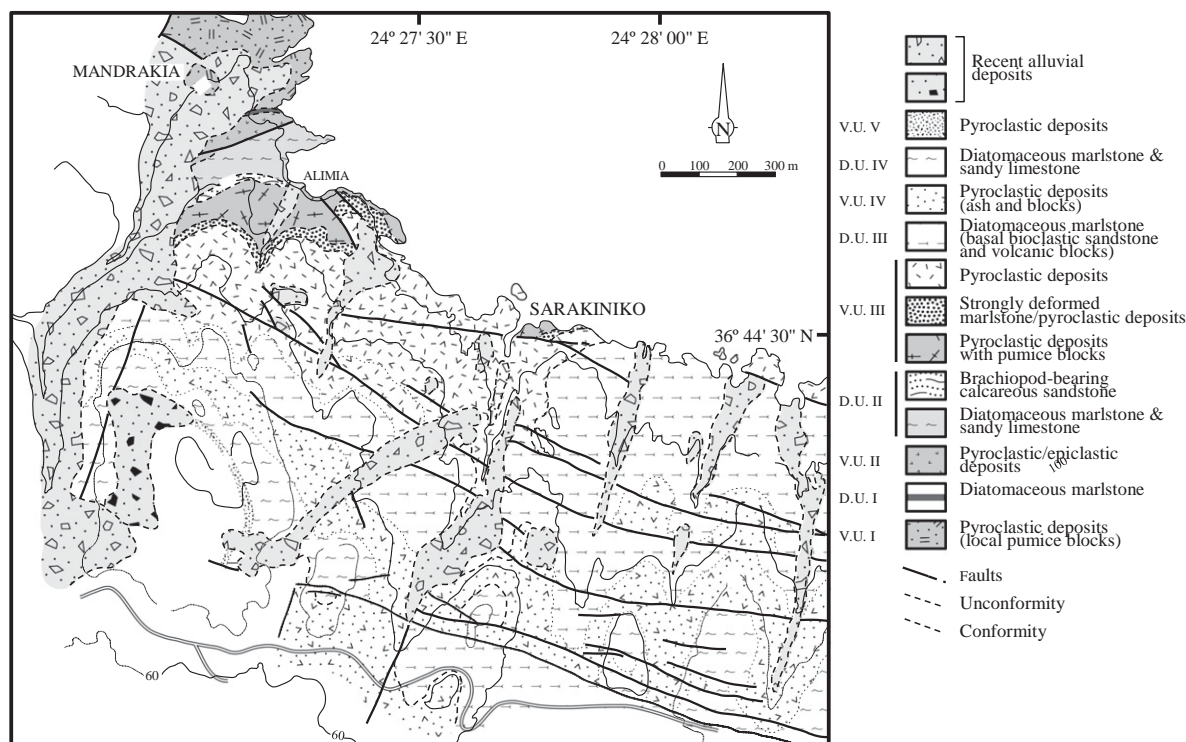


Fig. 2. Detailed map of the Mandrakia–Alimia–Sarakiniko area. Twelve lithological units representative of volcanoclastic and sedimentary deposits have been mapped. These units are unconformably overlain by recent alluvial sediments. The different volcanoclastic and diatomaceous sedimentary units are named as V.U. I to V (volcanic units) and D.U. I to IV (diatomaceous units) (see Fig. 3 for location of these units throughout a general lithostratigraphic log).

3. Materials and methods

The present study focuses on the diatomaceous marlstone and associated sedimentary facies that alternate with packages of volcanoclastic rocks in the northern part of Milos (Fig. 2). The stratigraphic succession reaches up to 300 m in thickness and is included in the “lower volcanoclastic series” (also named “basal pyroclastic series”) of Fytikas (1977). Rinaldi and Campos Venuti (2003) described these rocks as generally “marine fossiliferous sandstone”.

Mapping of the area at 1:5000 scale allowed for the reconstruction of the lithostratigraphic framework for the deposits. Such detailed mapping was needed in view of the complex tectonic structure of the area, characterised by a dense network of normal faults. Two main fault groups, oriented 15° and 115°, form the basic tectonic pattern together with a W–E stretched normal fault near Sarakiniko and some 80° oriented faults in the proximities of Mandrakia (Fig. 2). These faults define a subsiding area between Adamas, Sarakiniko, and the Zefiria Plain (Fig. 1) (Rinaldi and Campos Venuti, 2003).

Twelve superposed map units, covered unconformably by recent alluvial sediments (Fig. 2), have been differentiated. These map units can be integrated into a general lithostratigraphic column that exceeds 300 m thickness and comprises five lithologic units composed of volcanoclastic rocks and four lithological units that consist mainly of diatomaceous marlstone and sandy limestone (called ‘diatomite units’ in Fig. 3).

Eighty two samples were collected for petrographic analysis under polarised light microscope, 25 of them also analysed by scanning electron microscope (SEM) imaging (Jeol JSM-6400 and Hitachi 5400 field transmission apparatus). X-ray diffraction was used to determine mineral composition in powdered sandy limestone and diatomaceous marlstone. Chemical analysis of major elements in 35 samples was performed by X-ray fluorescence.

In addition, 28 samples were analysed for calcareous nannofossil content. Smear slides were prepared for each sample using standard

techniques (Perch-Nielsen, 1985). Analyses were performed using a Leica DMSP polarising light microscope at 1250 × magnification, by counting at least 300 specimens per sample; counts of index species were converted into percentages. For very rare species, e.g. discoasterids, up to 1500 fields of view were examined in randomly distributed longitudinal transverses per slide. Semiquantitative analysis in 15 fields of view was applied for the very small species such as

Gephyrocapsa spp. b3 µm and *Florisphaera profunda*. Zonal assignments of the nannofossil content follow the zonal scheme of Rio et al. (1990), incorporating updates by Lourens et al. (2004) and Raffi et al. (2006).

Twenty-three samples of diatomaceous marlstone rocks were collected and processed for fossil diatom study under SEM. Nine of them were not used for the study as they did not contain sufficient diatom forms. Distinction was made between subsamples derived from light and dark laminae in order to assess differences in the content of diatoms, clays and/or other components.

Twelve marlstone samples were washed through a 200 mesh sieve and analysed for their foraminiferal content under binocular microscope.

4. Lithostratigraphy

Nine lithostratigraphic units have been distinguished in the upper Pliocene–lower Pleistocene succession of northern Milos (Fig. 3). The units have been differentiated on the basis of the dominant lithologies that consist of (i) fossiliferous sedimentary rocks consisting of marlstone and limestone with varied amounts of reworked volcanic grains and (ii) volcanoclastic rocks mostly composed of pumiceous materials. The marlstone deposits are mainly diatomaceous and include a variety of diatom, foraminifera and calcareous nannofossil assemblages that contribute significantly to both palaeoenvironmental interpretation and dating of the stratigraphic succession.

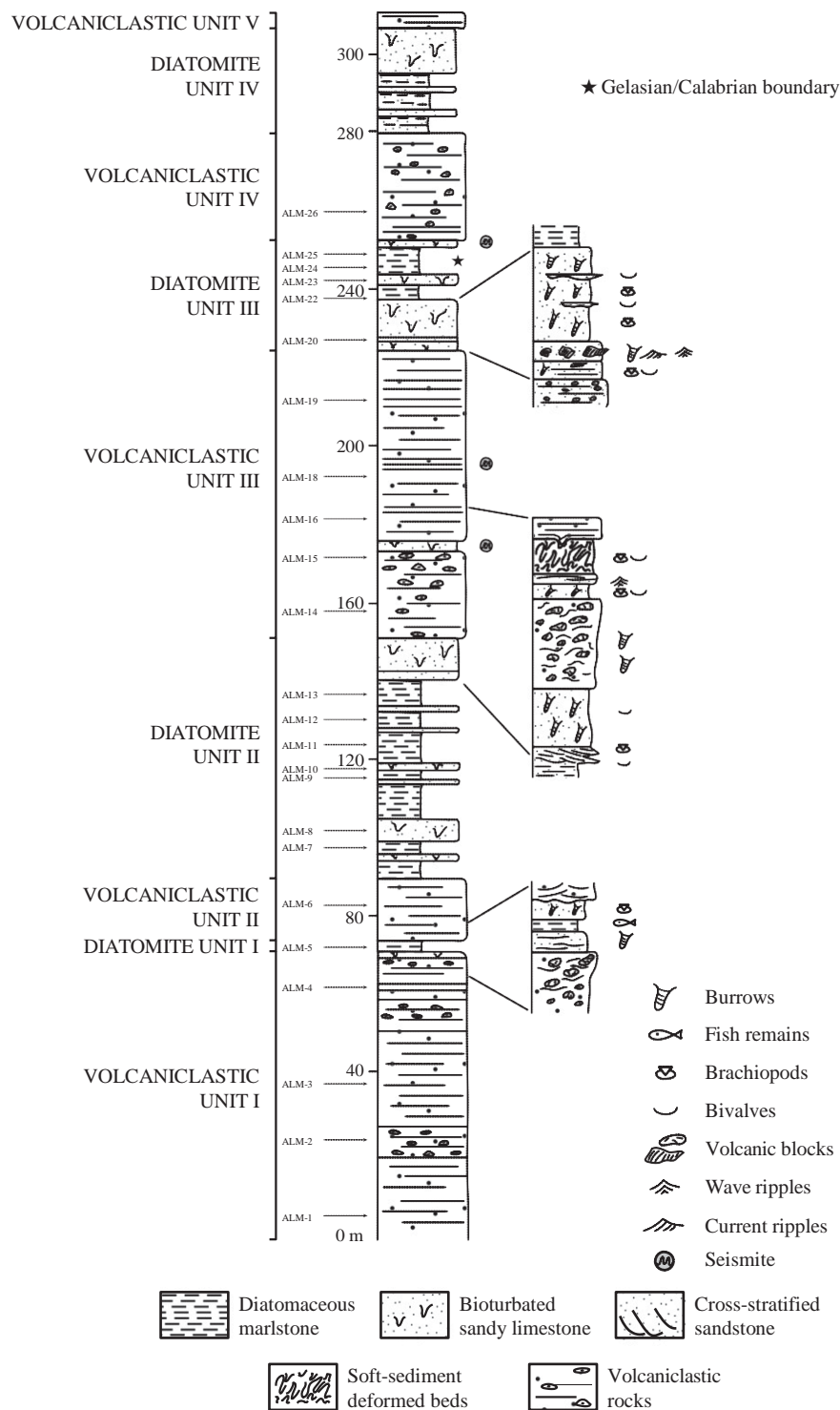


Fig. 3. General lithostratigraphic log showing the upper Pliocene–lower Pleistocene volcaniclastic and sedimentary units identified in the Alimia–Sarakiniko area, northern Milos. Shorter sections at right of the log show sedimentological details recognised in some units. Arrows at left of the log indicate location of micropalaeontological samples. Black star points out the Gelasian/Calabrian boundary within Diatomite Unit III.

4.1. Fossiliferous sedimentary rocks

Laminated diatomaceous marlstone alternating with sandy limestone constitutes the most common sedimentary facies association in all diatomite units throughout the whole succession. In total, 14 sedimentary cycles formed of diatomaceous marlstone and sandy limestone beds were measured. Thicknesses of the sedimentary couplets are variable, ranging from 2.5 to 10.5 m. Likewise,

thicknesses of the intervening diatomaceous marlstone and sandy limestone beds that form each cycle are also variable. The thickest, up to 9.5 m, diatomaceous marlstone deposit was recognised in Diatomite Unit II (Fig. 4). Laminae in the diatomaceous marlstone are defined by submillimetre-thick lithic/biogenic couplets (sensu Sancetta, 1996) (Fig. 5A, B). Usually, the diatomaceous marlstone forms the lower part of the sedimentary cycles and the contact with the underlying sandy limestone is sharp. Upward transition



Fig. 4. Outcrop showing laminated diatomaceous marlstone from Diatomite Unit II. Thickness of the bed is up 9.5 m and the section top is located at right of the picture. Both the bottom and the top of the diatomaceous deposit are marked by sandy limestone beds (arrows).

from diatomaceous marlstone to sandy limestone is rapid gradational and is marked by burrow traces (Fig. 6) that become largely developed in the sandy limestone in the upper part of each sedimentary cycle.

Cross-stratified, brachiopod-rich (*Terebratula* spp.) sandstone beds (Fig. 7) occur in the upper part of Diatomite Unit II (Fig. 3). A wave-rippled sandstone and siltstone bed showing well-developed burrow traces (Fig. 8) occurs at the base of Diatomite Unit III (Fig. 3). Although these lithofacies are only locally present in the succession, they are indicative of relevant stratigraphic events of the geological evolution of Milos during the late Pliocene and early Pleistocene (see discussion below).

Table 1 provides a description and interpretation of the several lithofacies distinguished from fossiliferous sedimentary rocks in the stratigraphic succession of northern Milos.

4.2. Volcaniclastic rocks

In this paper, the term ‘volcaniclastic’ is used in a simple descriptive way to name rocks composed chiefly of grains of volcanic origin, derived from contemporaneous volcanicity (Tucker, 2001) and that result from any mechanism of fragmentation (Vincent, 2000). The stratigraphic section in northern Milos records mainly volcaniclastic rocks related to submarine felsic cryptodome–pumice cone volcanoes (Stewart and McPhie, 2006). Products from this type of submarine volcanism are largely represented by white to cream pumiceous deposits with subordinate occurrence of dark lithic fragments that record a long history of explosive eruptions (Rinaldi and Campos Venuti, 2003).

The five volcaniclastic units distinguished throughout the upper Pliocene–lower Pleistocene succession of northern Milos (Fig. 3) are composed of volcaniclastic rocks that display features indicative of deposition in a submarine setting (Table 2). Maximum thickness of the volcaniclastic units was measured in Volcaniclastic Unit III, where three superposed packages of volcanic products bounded by unconformities and/or truncations reach up to 75 m (Fig. 3).

Sedimentary structure, scarce fossil remains and burrow traces, and the presence of fossiliferous deposits above and below the pumice packages strongly suggest accumulation under dominantly below-wave-base conditions. In this setting, the volcanic products were

distributed by submarine currents and/or gravitational flow processes close to the volcanic submarine source centres (Table 2).

The structure of the volcaniclastic rocks varies from massive to well-bedded. Massive volcaniclastic deposits usually formed of coarse breccia occur in Volcaniclastic Units I, II and III (Fig. 9A) whilst Volcaniclastic Units IV and V are composed of better stratified deposits (Fig. 9B). These changes of volcaniclastic units up succession can be interpreted as reflecting the evolution from submarine to very shallow even subaerial volcanism throughout the late Pliocene to Pleistocene in most of Milos Island, an idea already suggested by Stewart and McPhie (2006).

Sand- to silt-sized volcanic grains are a common component of the fossiliferous sedimentary rocks alternating with volcaniclastic deposits in northern Milos. Besides this occurrence, big volcanic blocks ranging from 0.20 to 4.40 m in diameter occur isolated and aligned at the base of Diatomite Unit III (Fig. 3). The volcanic blocks overlie wave-rippled sandstone and siltstone deposits and together form a key-bed that can be followed for a few hundreds of metres east of the Sarakiniko canyon.

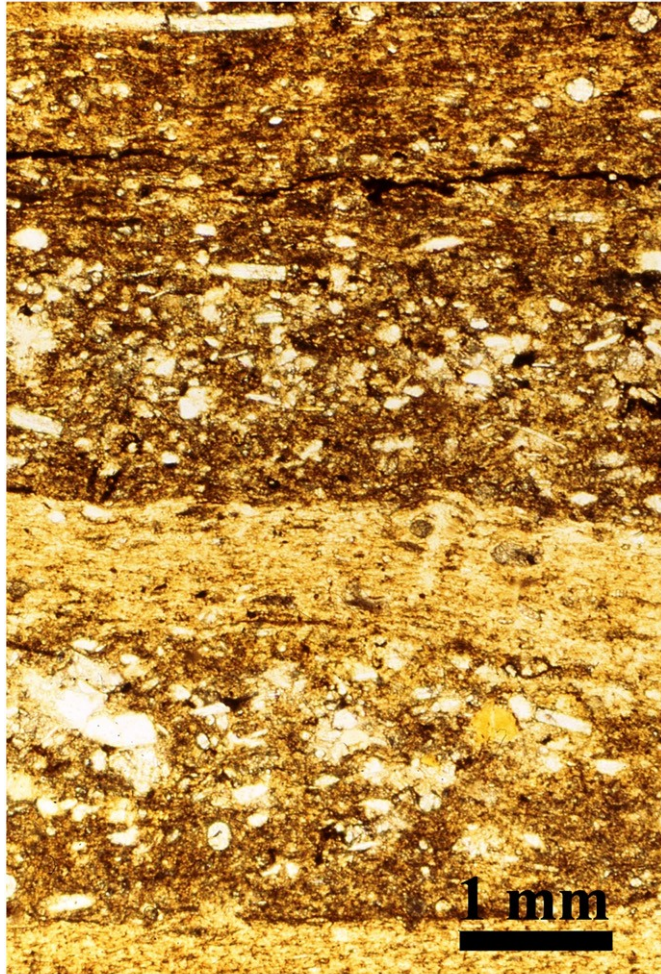
4.3. Seismic imprint resulting in soft-sediment structures

Both fossiliferous sedimentary rocks and volcaniclastic deposits display soft-sediment deformation structures. The deformation structures consist of i) burrowing-related deformation that mainly affects laminated diatomaceous marlstone, ii) deformation structures due to loading (Owen, 1996), and iii) soft-sediment deformation structures of probable seismic origin, i.e., seismites (Collinson, 1994).

Loading is considered the usual triggering mechanism of soft-sediment deformation structures in the volcaniclastic deposits of northern Milos. Disturbance of well-bedded fine-grained pumiceous deposits by loading of coarse-grained, rapidly accumulated volcaniclastic material under subaqueous conditions resulted in convolute bedding and flame and pillow-like structures (Fig. 10).

Soft-sediment deformation structures interpreted as seismically induced are present at certain intervals of the upper Pliocene–lower Pleistocene succession. At least three main horizons, occurring at 175 m, 195 m and 255 m from the bottom of the section (Fig. 3), display clear earthquake-related deformation structures. The seismite beds are composed both of fossiliferous diatomaceous marlstone

A



B

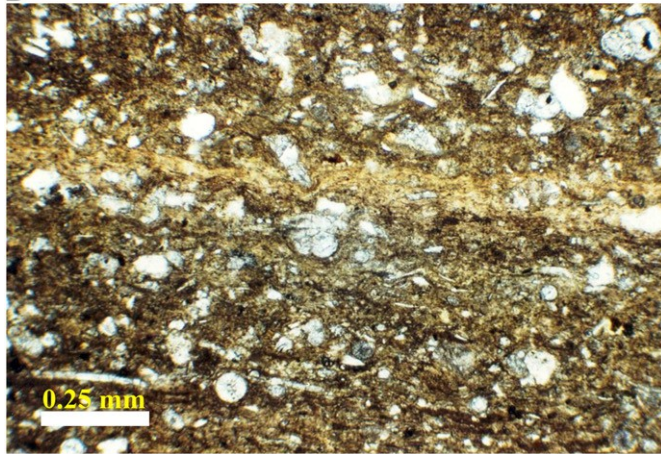


Fig. 5. A: Photomicrograph of diatomaceous marlstone. Dark lithic laminae contain abundant grains of volcanic origin and exhibit a sharp contact with underlying lighter biogenic laminae composed mainly of diatom frustules. B: Volcanic grains mixed with forams and sponge spicules in lithic laminae.

(Fig. 11) and laminated pumice ash. Each of the three strongly deformed beds is overlain by volcanoclastic units that record new episodes of explosive volcanism. This stratigraphic relationship supports that the deformation of the underlying deposits was triggered by earthquakes taking place prior to eruptive events (Jones and Omoto, 2000; Schminke, 2004).

5. Micropalaeontology and age framework of the Alimia–Sarakiniko sequence

Results from the calcareous nannofossil analysis of diatomaceous marlstone samples (Fig. 3) are summarised in Table 4. Samples ALM2a to ALM6 from Diatomite Unit I and ALM14 to ALM20 from Diatomite Unit II were barren while sample ALM9 contained only diatom microfossils. The rest of the collected samples contained both diatom- and calcareous nannofossil-rich assemblages. Quantitative analysis of samples ALM7 to ALM12 from Diatomite Unit II shows common *Helicosphaera sellii*, *Calcidiscus macintyreii*, *Pseudoemiliana lacunosa*, *Braarudosphaera bigelowii* and very rare small *Gephyrocapsa* spp. (Fig. 12). *Discoaster* spp. are also very rare, represented by few specimens of *D. asymmetricus*, *D. tamalis* and *D. triradiatus* per sample (Table 4; Plate I). Semiquantitative analysis documented abundant *Florisphaera profunda*. Sample ALM22 contains *H. sellii*, *C. macintyreii*, *P. lacunosa* and abundant small *Gephyrocapsa* spp. However, discoasterids and normal size *gephyrocapsids* (*Gephyrocapsa* spp. > 4 µm) were not detected. The first unambiguous representatives of > 4 µm *Gephyrocapsa* spp. occur in samples ALM23–26 from Diatomite Unit III (Plate I; Fig. 3).

A rich foraminiferal assemblage (Table 4) composed of *Globigerina bulloides*, *G. falconensis*, *G. quinqueloba*, *Globigerinoides ruber*, *Neoglobobulimina pachyderma*, *Orbulina universa* and *Lobatula lobatula* is a feature of the samples from Diatomite Unit II. However, no traces of *Sphaeroidinellopsis* spp. have been recorded. Foraminiferal assemblages in Diatomite Unit III are dominated by *Globigerinoides saculifer*, *Globigerinella aequilateralis*, and *Globorotalia inflata*. Samples collected in Diatomite Unit IV show abundant benthic foraminifers but very sparse planktonic forms (*Globigerina bulloides*, *G. quinqueloba*, *G. falconensis*, *Globigerinoides ruber* and *Neoglobobulimina pachyderma*). The diatom assemblages (Table 4) from Diatomite Unit I contain abundant *Rophadolia*, *Actinocyclus* spp., and *Rhizosolenia* and *Grammatophora* in both light and dark laminae whilst *Coscinodiscus* and *Thalassionema nitzschioides* are more common in the light laminae. Diatomaceous sediments from Diatomite Unit II show a variety of diatom forms with abundant *Rophadolia*, *Thalassionema*, *Rhizosolenia*, *Thalassiosira*, *Nitzschia*, *Hemidiscus*, *Cyclotella*, and *Actinocyclus*, mostly in the light laminae. Samples collected from Diatomite Units III and IV contain a similar diatom assemblage with abundant *Stephanopyxis* and *Amphora* forms.

Several beds exposed in the area are well-known at a regional scale because of both richness and good preservation of macrofossils. This is the case for a palaeontological site close to Sarakiniko (Sonder, 1924) that yields a rich fossil association of bivalves (*Chlamys* spp., *Pecten*, *Isocardia*, *Solecardia*, *Pinna*, *Ostrea*, *Chama*, *Lucinopsis*), scaphopods (*Dentalium*), gastropods (*Scala*), brachiopods (*Terebratula* spp.), echinoids (*Arbacia*, *Psammechinus*, *Schizaster*, *Lytechinus*, *Brissopsis*, *Prostagantus*), and barnacles (Table 4).

Fytikas et al. (1976, 1986) and Fytikas and Vougioukalakis (1995) indicated that accumulation of the “lower volcanoclastic series” possibly started during the middle Pliocene (~3.4 ± 3.0 Ma). K/Ar dating of a non-juvenile rhyolite clast in submarine pumice breccia suggested a maximum age of 3.08 ± 0.14 Ma (Fytikas et al., 1986). An upper age limit for the submarine pumice breccias at ~2.66 ± 0.07 Ma was provided by U/Pb dating of the Filakopi Pumice Breccia (Stewart and McPhie, 2004) and the volcanic activity in the northern part of Milos has been more or less continuous since then (Stewart and McPhie, 2006). SHRIMP U–Pb dating of zircon in one of the oldest subaerial dacite domes (Stewart and McPhie, 2006) yielded an age of 1.44 ± 0.08 Ma. This suggests that the subaerial part of the volcanic succession in northern Milos Island began at that time in response to a combination of volcanic constructional processes and fault-controlled volcano-tectonic uplift (Stewart and McPhie, 2006). Additional age information is provided by a radiometric age of 1.85 Ma on biotite from a dacite pumice clast collected in the pyroclastic



Fig. 6. Outcrop view of massive, strongly burrowed sandy limestone capping a diatomaceous marlstone-sandy limestone cycle at the top of Diatomite Unit III. Hammer for scale is 30 cm long.

deposits of this series cropping out near Sarakiniko (Fytikas et al., 1986). Kondopoulou and Pavlides (1990) determined an age of 1.8 Ma for an andesite lava flow (Korakia Andesite of Stewart and McPhie, 2003a) overlying the Sarakiniko deposits. A younger radiometric age (1.6 Ma) for the lava domes overlying the lower series to the east of the study area was provided by Fytikas et al. (1986), which yields an upper age limit for the succession analysed in northern Milos.

Regarding the fossiliferous sedimentary rocks of northern Milos, Sonder (1924) initially suggested a late Pliocene age for the rich macrofossil assemblage in calcareous beds occurring near Sarakiniko (see fossil content in a previous paragraph). Later on, Fytikas (1977) suggested a possible middle Pliocene age for those beds on the basis of planktonic foraminiferal assemblages, although these were lacking

biostratigraphic indices. According to the new evidence provided by calcareous nannofossils from samples collected in the lower part of Diatomite Unit III (Fig. 3), the diatomaceous and calcareous deposits of this unit are biostratigraphically correlated with MNN19a–MNN19b nannofossil biozones, spanning a time interval between 1.95 and 1.73 Ma (Lourens et al., 2004), so their age must be changed to Gelasian/Calabrian (formerly late Pliocene, currently early Pleistocene; Gibbard et al., 2009; Papanikolaou et al., 2011). This fits well earlier work by Frydas (1992, 1996a) who on the basis of silicoflagellates and diatoms dated the SE-Adamas fossiliferous site as early Pleistocene. Unequivocal stratigraphic correlation of this fossiliferous site with the third uppermost diatomaceous marlstone-sandy limestone cycle of Diatomite Unit III can be established by tracing the cyclically arranged beds from Sarakiniko to SE Adamas.



Fig. 7. Cross-stratified, brachiopod-rich (*Terebratula* spp.) sandstone showing at least three superimposed foreset beds interpreted as foreshore deposits. Dip is to the east (left of the outcrop); these beds occur near the top of Diatomite Unit II. Hammer for scale is 35 cm long.



Fig. 8. Wave-rippled sandstone and siltstone showing parallel to oblique oriented burrow

traces (*Thalassinoides*).

The rest of the stratigraphic succession studied in northern Milos, including Diatomite Unit IV, is correlated to nannofossil biozone MNN19b of early Calabrian age.

The biostratigraphic assignment of Diatomite Unit II to nannofossil biozone MNN16a (Rio et al., 1990), particularly in between the highest occurrence of *Discoaster asymmetricus* (2.83 Ma, Lourens et al., 2004) and the highest occurrence of *Sphaeroidinellopsis* spp. (3.19 Ma, Lourens et al., 2004) supports a late Pliocene (Piacenzian) age for the lower part of the Alimia–Sarakiniko stratigraphic succession.

6. Palaeoenvironmental reconstruction and major events during the late Pliocene–early Pleistocene in northern Milos

Except for some horizons of Diatomite Unit II, where cross-stratified, brachiopod-rich (*Terebratula* spp.) sandstone shows features indicative of very shallow-marine depositional conditions, most of the upper Pliocene–lower Pleistocene rocks in northern Milos formed mostly.

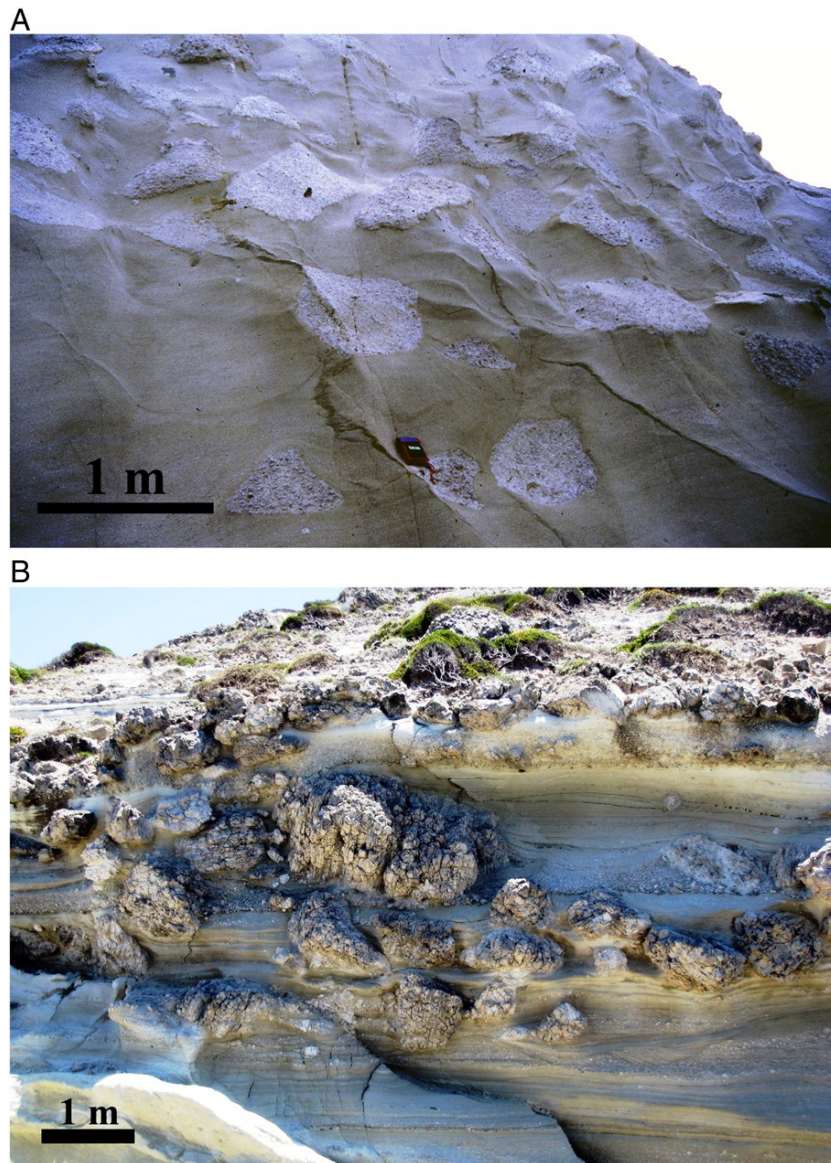


Fig. 9. A: Outcrop of coarse pumice breccia (lower part of Volcaniclastic Unit III) showing a remarkable bimodal grain-size. Metre-size, angular pumice blocks are imbedded in laminated pumice ash. Compass case used for scale is 15 cm high. The outcrop is located about 200 m west of Sarakiniko. B: Outcrop showing pumice blocks included in crudely laminated fine-grained pumice (Volcaniclastic Unit IV); the outcrop is located east of Sarakiniko.

Table 1

Description and interpretation of fossiliferous sedimentary rocks in the upper Pliocene–lower Pleistocene succession of northern Milos.

Facies	Description	Interpretation
<p><i>Laminated diatomaceous marlstone</i></p> <p>Present in all diatomite units. Fourteen diatomaceous marlstone horizons alternating with massive sandy limestone were measured in the section. Bed thickness ranges 1.20–9.50 m.</p>	<p>Sedimentary features and bioclastic components:</p> <p>Millimetre-thick laminated to locally banded, white to light-grey beds. Laminae are defined by submillimetre-thick lithic/biogenic couplets (Fig. 5A).</p> <p>Dark lithic couplets composed of fine-grained sand and silt, medium- to poorly- sorted volcanic glass fragments, with minor quartz and feldspar grains in clayey– calcareous micrite. Planktonic and benthic foraminifera, ostracod shells, and sponge spicules occur mixed with the siliciclastic grains (Fig. 5B).</p> <p>Light biogenic laminae formed of dense aggregates of large, usually broken frustules of planktonic diatoms and siliceous sponge spicules.</p> <p>Occurrence of both complete skeletons and scales from undetermined fish species. Presence of large, isolated burrow patches (<i>Ophiomorpha</i>? sp.) leading to local soft- sediment deformation.</p> <p>Intercalations of up to 2 cm thick layers of massive to slightly graded marlstone formed of clay aggregates, lithic, and bioclastic grains floating in micrite matrix. Thicker beds of the massive marlstone occur at the gradational transition into sandy limestone.</p> <p>Chemical and mineralogical composition:</p> <p>Whole-rock SiO₂ concentrations variable from 35 to 71% SiO₂ (Table 3). SiO₂/ Al₂O₃ ratio ranging from 5% to 28%.</p> <p>Opal-A as common constituent of the laminae, specially in biogenic couplets; lesser amount of opal-A in the dark lithic couplets. No evidence of transformation from opal-A to opal-CT and/or quartz.</p> <p>Calcite percentage ranging from 0 to 70% (Table 3). Dolomite does not exceed 5%.</p>	<p>Deposition below the zone of wave influence. Alternating episodes of detrital input followed by periods of maximal, probably seasonally- controlled productivity.</p> <p>Depositional setting characterized by oxygen-deficient bottom waters resulting from water stratification in a partially closed, relatively shallow sea. Palaeogeographic features determined by development of silled basins (Fig. 13).</p> <p>Input of lithic detritus by dilute turbidite flows to the basin (coincident with periods of runoff and/or aeolian transport). Terrigenous influx related to reworking of pre-existing basin deposits.</p> <p>Diatom and calcareous nannofossil assemblages (Table 4; Fig. 11) characteristic of high productivity periods. Biosiliceous productivity probably related to local upwelling of nutrient-rich waters and/or input of terrestrial nutrients.</p> <p>Occurrence of some calcareous nannofossils, i.e. <i>Braarudosphaera</i> spp., indicative of freshwater input during deposition of the diatomaceous marlstone and proximity of land source areas.</p> <p>Large <i>Ophiomorpha</i>? sp. burrow traces interpreted as living conduits (Domichnia) of decapod crustaceans. Local development of burrowing infauna related to episodes of improved benthic oxygenation in a depositional environment characterised by oxygen-deficient conditions.</p>
<p><i>Massive sandy limestone</i></p> <p>Present in all diatomite units, usually alternating with laminated marlstone. Up to 20 m thick sequences of massive sandy limestone occur in Diatomite Units II and III.</p>	<p>Strongly burrowed sandy limestone beds. No presence of current and/or wave generated sedimentary structures.</p> <p>Percentage of siliciclastic sand grains (volcanic glass, quartz, and feldspar) ranging from 15 to 40%. Mixing with bivalve, echinoid, brachiopod, benthic and planktonic forams imbedded in calcareous micrite groundmass.</p> <p>Large variety of macro and microfossils (mainly benthic forms). Local occurrence of small oyster patch-reefs.</p>	<p>Deposition in a shallow self to shoreface environment characterized by well-oxygenated conditions as indicated by predominance of benthic fossil forms, abundance of siliciclastic grains and lack of sedimentary structures characteristic of turbidity currents.</p> <p>Burrowing due to bivalves, echinoids and brachiopods.</p>
<p><i>Cross-stratified, brachiopod-rich (Terebratula spp.) sandstone</i></p> <p>Present in the upper part of Diatomite Unit II. Formed of foreset beds dipping ~20° ESE.</p>	<p>Occurrence as a package of superimposed 30 cm thick foreset beds (total thickness of the cross-bedded deposit is 1.50 m). The foresets extend up to 20 m down-dip passing laterally into burrowed sandy limestone. Gently sloped, large channels observable in cross-section.</p> <p>Abundant casts of <i>Terebratula</i> ssp. in sandstone formed of well-sorted, rounded siliciclastic (quartz, volcanic fragments), peloids, and bioclastic (benthic foraminifera, bivalves, echinoids) grains.</p>	<p>Deposition in a beach environment (foreshore facies).</p> <p>Terrigenous material supplied by both subaerial and submerged volcanic outcrops.</p> <p>Bioclasts derived mainly from benthic macrofauna living in the littoral zone.</p> <p>Facies transition into burrowed sandy limestone indicative of rapid change from foreshore to shoreface sub-environments.</p>
<p><i>Wave-rippled sandstone and siltstone</i></p> <p>Present in the lower part of Diatomite Unit III. Key-bed (up to 0.80 m thick) traceable for a few hundred metres east of Sarakiniko.</p>	<p>Oblique to horizontally laminated, wavy-rippled bioclastic sandstone alternating with silty marlstone. Sub-rounded, moderately to well-sorted, medium- to fine-grained sandstone and siltstone mainly formed of quartz, volcanic grains, and bioclasts (bivalves, echinoids, benthic forams).</p> <p>Common occurrence of burrowing (<i>Thalassinoides</i>), both oblique and parallel to the sandstone layers. Burrow traces display two different sizes: most common type is 1–2 cm wide; less common burrow traces are 3–4 cm wide.</p>	<p>Deposition under relatively low-energy conditions in a proximal/coastal environment.</p> <p>Burrow traces representative of both vertical and horizontal living conduits of estomatopod crustaceans. Small size of the burrows supports deposition in a very shallow-water environment.</p>

Table 2
Description and interpretation of volcanoclastic rocks in the upper Pliocene–lower Pleistocene succession of northern Milos.

Facies	Description	Interpretation
<p><i>Massive coarse pumice breccia</i></p> <p>Present in V.U. I, II and III.</p>	<p>Massive, poorly sorted deposit composed of boulder (up to 3 m) to cobble pumice clasts set in fine-grained pumiceous and shard-rich matrix (Fig. 8A). The pumice clasts mainly composed of aggregates of rhyolitic shards and vesicular glass. Matrix-supported fabric dominant. Remarkable bimodal grain-size distribution.</p> <p>Pumice clasts usually display reverse grading whereas matrix is internally normally graded. Subangular to subrounded pumice clasts displaying internal polyhedral joints and quenched margins. Dense lithic clasts minor or absent.</p> <p>Diffusely stratified pumice to shard-rich matrix usually displaying internal normal grading. Lower contacts are gradational whilst upper contacts are commonly sharp and planar. Maximum measured thickness 23 m. Low-angle truncation surfaces and scouring between sets of laminae. Local pumice blocks associated with crescent scours. Mantling of pumice blocks by ash laminae.</p> <p>Local burrowing (cm- to dm-sized burrow traces) by macrobenthic infauna.</p>	<p>Submarine water-settled pumice deposit resulting from explosive rhyolitic eruptions. Facies similar to the pumice breccia described in Filakopi by Stewart and McPhie (2004).</p> <p>Settling of coarse pumice clasts from suspension and progressive infilling by fine pumice ash. Pumice clasts were freshly erupted (juvenile clasts). Quenched margins of coarse pumice clasts indicative of minimal abrasion during transport and deposition.</p> <p>Accumulation in relatively shallow-marine but dominantly below-wave- base setting. The shallow-marine depositional conditions are also indicated by occurrence of sparse infaunal burrowing, benthic fossils and stratigraphic relationship with shallow-water fossiliferous sedimentary rocks.</p> <p>Remobilisation of pumice by gravity currents and local mass-flow processes, i.e. sliding and slumping of pumice bed packages.</p>
<p><i>Stratified fine-grained pumice</i></p> <p>Present in V.U. II and III.</p>	<p>Well-bedded pumice-rich deposit showing crudely stratified or laminated internal structure. Moderately sorted pumice pebbles (up to 4 cm) and glass shards are dominant components. Dense lithic clasts locally present at the lower part of some beds. Beds show sharp lower and upper contacts (Fig. 10) and internally display normal to reverse grading. Bed thickness is variable (20–80 cm). Rapid bed thinning is common, occasionally resulting in bed truncation.</p> <p>Soft-sediment deformation structures are common, especially in finer-grained, shard-rich deposits (Fig. 10).</p>	<p>Deposition of pumice and other juvenile volcanic clasts mainly resulting from water-settling processes.</p> <p>Well-developed bedding indicative of punctuated submarine rhyolitic eruptions. Fine-grained texture and sorting indicative of accumulation in distal areas from the vent volcanic source.</p>
<p><i>Stratified to laminated ash and pumice blocks</i></p> <p>Present in V.U. IV.</p>	<p>Thinly bedded to laminated ash composed of pumice fragments and glass shards with pumice block (0.30–2.40 m) concentrations (Fig. 9B). Marked bimodal fabric. Internal structure of the pumiceous ash beds (commonly centimetres thick) marked by diffuse, plane-parallel and low-angle cross-beds. Local small-scale discordances and truncations. Normally graded pumice beds.</p> <p>Bedding distorted by occurrence of pumice blocks displaying internal polyhedral joints. Mantling of pumice blocks by ash laminae.</p>	<p>Deposition resulted from mixing of water-supported gravity flows of volcanoclastic debris and settling from suspension of submarine rhyolitic volcanic products. The facies is similar to medial facies of the volcanoclastic apron described by Rinaldi and Campos Venuti (2003).</p> <p>Bimodal fabric related to the different behaviours of pumice blocks to float within the water column, then sinking when density of blocks increases by water absorption.</p>
<p><i>Volcanic blocks resting on terrigenous deposits</i></p> <p>Present in the lower part of D.U. III</p>	<p>The volcanic blocks (0.20–4.40 m) occur aligned at a same stratigraphic level, resting on wave-rippled sandstone and siltstone (Table 1) that show local soft- sediment deformation due to loading of the volcanic blocks.</p> <p>Compositionally the volcanic blocks are dacite–andesite and display internal fluidal structure.</p>	<p>Drift of volcanic blocks after fragmentation of exposed dacite–andesite lava flows accumulated in a coastal environment. Accumulation of the volcanic blocks near the coastline as indicated by wave-rippled terrigenous deposits at the base of the blocks.</p>

Table 3

Chemical composition (% oxides) and calcite and dolomite contents of laminated diatomaceous marlstone. Samples SRK 01 to 30 and SRK 907–908 were analysed at the Instituto di Mineralogia e Geochimica of the Palermo University; data for samples MilosV1 to 5, corresponding to volcanoclastic material, were obtained at the laboratory of the TITAN Cement Co, in Athens. (MilosV1: perlite clast from V.U. III; MilosV2: pumice boulder in wave-rippled sandstone from D.U. III; MilosV3: rhyolite lava from Fyriplaka; MilosV4: andesitic tuff; MilosV5: rhyodacitic tuff). Calcite and dolomite contents were determined at the Laboratory of Mineralogy and Geochemistry of the University Autonoma of Madrid.

Sample	SiO ₂	TiO ₂	Al ₂ O ₃	Fe ₂ O ₃	MnO	CaO	Mgo	Na ₂ O	K ₂ O	P ₂ O ₅	L.O.I.	Calcite %	Dolomite %
SRK 01	71.01	0.19	4.26	2.82	0.05	0.05	0.80	1.53	0.61	0.02	18.66	—	—
SRK 02	69.65	0.10	2.34	1.66	0.07	0.00	0.45	2.44	0.30	0.02	22.99	—	—
SRK 04	40.87	0.18	5.51	2.36	0.07	5.51	7.41	2.19	0.71	0.11	35.08	—	17
SRK 05	42.13	0.10	3.08	1.10	0.04	6.39	6.88	1.40	0.49	0.17	38.22	—	16
SRK 06	70.74	0.16	2.52	4.30	0.23	1.35	0.05	2.24	0.39	0.00	18.02	—	—
SRK 07	42.82	0.16	4.13	3.96	0.04	7.29	4.97	1.02	0.64	0.06	34.90	—	15
SRK 08	35.83	0.15	3.67	1.68	0.05	13.61	6.15	1.02	0.65	0.12	37.06	10	16
SRK 09	39.46	0.18	5.15	2.24	0.05	13.53	4.53	1.28	0.68	0.14	32.75	16	15
SRK 10	53.81	0.19	4.33	2.28	0.05	11.89	2.98	1.02	0.71	0.12	22.62	11	8
SRK 11	45.35	0.11	2.67	1.63	0.07	14.25	2.45	1.00	0.43	0.11	31.94	20	8
SRK 13	54.48	0.11	2.78	2.10	0.03	4.70	2.30	1.29	0.45	0.03	31.75	5	8
SRK 14	48.87	0.15	3.02	3.45	0.05	11.17	3.98	0.99	0.56	0.03	27.65	13	14
SRK 15	61.47	0.20	4.20	3.98	0.04	11.25	0.81	0.98	0.71	0.03	16.34	20	—
SRK 16	35.08	0.09	2.51	1.37	0.03	16.05	0.41	1.67	0.31	0.03	42.44	29	—
SRK 17	68.53	0.16	3.25	2.26	0.05	8.30	1.11	0.98	0.59	0.14	14.65	14	b5
SRK 17b	28.54	0.11	3.94	1.17	0.06	12.64	4.70	1.57	0.48	0.11	46.68	11	18
SRK 18	62.26	0.15	3.27	2.76	0.04	11.60	0.62	0.97	0.56	0.05	17.73	20	—
SRK 19	57.49	0.15	3.54	2.93	0.06	9.91	1.52	1.13	0.56	0.09	22.62	15	5
SRK 20	47.14	0.17	4.69	2.48	0.07	12.03	1.79	1.18	0.59	0.05	29.82	20	5
SRK 21	43.18	0.13	3.28	1.86	0.04	11.14	5.53	1.05	0.76	0.10	32.91	19	b5
SRK 22	57.86	0.40	11.02	5.91	0.05	7.47	2.74	0.98	1.98	0.02	11.59	8	9
SRK 28	38.32	0.18	7.23	2.22	0.06	16.80	2.24	1.18	1.38	0.05	30.36	28	b5
SRK 38	55.08	0.25	6.75	3.83	0.05	12.58	1.39	0.98	1.11	0.03	17.96	20	b5
SRK 39	53.77	0.13	2.69	2.71	0.08	9.04	0.00	2.46	0.43	0.03	28.86	17	—
SRK 41	49.77	0.22	8.08	3.65	0.04	13.32	1.75	1.04	1.58	0.02	20.52	22	b5
SRK 42	48.77	0.18	5.91	2.60	0.08	14.88	0.00	1.50	1.12	0.02	24.94	24	—
SRK 45	63.67	0.15	3.49	3.83	0.08	6.74	0.04	1.86	0.55	0.02	19.58	11	—
SRK 46	57.77	0.14	3.75	2.61	0.06	12.06	0.42	1.38	0.52	0.01	21.26	20	—
SRK 907	45.14	0.10	4.47	1.72	0.03	11.57	0.36	3.25	0.60	0.07	32.68	18	—
SRK 908	57.23	0.18	5.04	1.62	0.05	13.72	1.83	0.99	0.11	0.10	19.14	21	b5
MilosV1	71.47	n.d.	14.26	1.79	n.d.	1.87	0.61	2.37	3.05	0.12	4.70	—	—
MilosV2	65.22	n.d.	15.22	3.50	n.d.	3.52	1.15	3.62	2.66	0.17	4.02	—	—
MilosV3	73.48	n.d.	13.27	1.49	n.d.	1.53	0.64	3.74	3.78	0.02	1.89	—	—
MilosV4	59.86	n.d.	15.63	5.31	n.d.	6.54	1.48	5.66	1.10	n.d.	3.58	—	—
MilosV5	72.14	n.d.	14.95	1.88	n.d.	1.84	0.55	2.33	3.51	n.d.	3.30	—	—

n.d.: not determined.

in submarine depositional environments, from shoreface to basinal. The occurrence of burrowing ichnofacies in laminated diatomaceous marlstone points to episodes of improved benthic oxygenation in sedimentary facies indicative of a generally oxygen-deficient

setting. This feature, together with the common cyclic association of laminated marlstone and burrowed sandy limestone, suggests that the basins were just some tens to a few hundreds of metres deep.



Fig. 10. Convolute bedding in fine-grained ash pumice deposits (lower part of Volcaniclastic Unit III in Sarakiniko). Lens cap for scale is 7 cm.



Fig. 11. Soft-sediment deformation of fossiliferous/pumiceous marlstone attributed to earthquakes (lower part of Volcaniclastic Unit III). The marlstone beds show a sharp, well-defined contact over fine-grained volcaniclastic deposits. Over the contact, the marlstone becomes progressively deformed. Hammer is 30 cm long.

Some palaeoecological differences during deposition of diatomite units can be determined on the basis of micropalaeontological contents. Thus, Diatomite Unit II is marked by a high content of lower photic zone nannofossil species *Florisphaera profunda* (Okada and Honjo, 1973) that has proven to be a very reliable proxy to locate the nutricline–thermocline level (Molfin and McIntyre, 1990) indicating marked stratification of the water column and low productivity within the surface layer (e.g. Castradori, 1993). The presence of *Braarudosphaera* spp. points to fresh-water input during deposition of the diatomaceous marlstone (Negri and Giunta, 2001; Triantaphyllou et al., 2009a, 2009b, 2010). For Diatomite Unit III, high abundance

of small nannofossil *Gephyrocapsa* spp. along with the presence of planktonic foraminifer *G. inflata* are indicative of a marine environment characterised by highly productive cool waters (e.g. Triantaphyllou et al., 2010).

Rhyolitic intrusions resulting in felsic cryptodome–pumice cone volcanoes (Stewart and McPhie, 2006) accounted for vast accumulation of coarse- to fine-grained pumice deposits that formed shoaling areas on seafloor. The resulting likely palaeogeography is a number of silled basins where laminated diatomaceous marlstone accumulated (Fig. 13). Extensive reworking of volcanic grains, mainly glass shards, by shallow marine currents and gravity flows is recorded

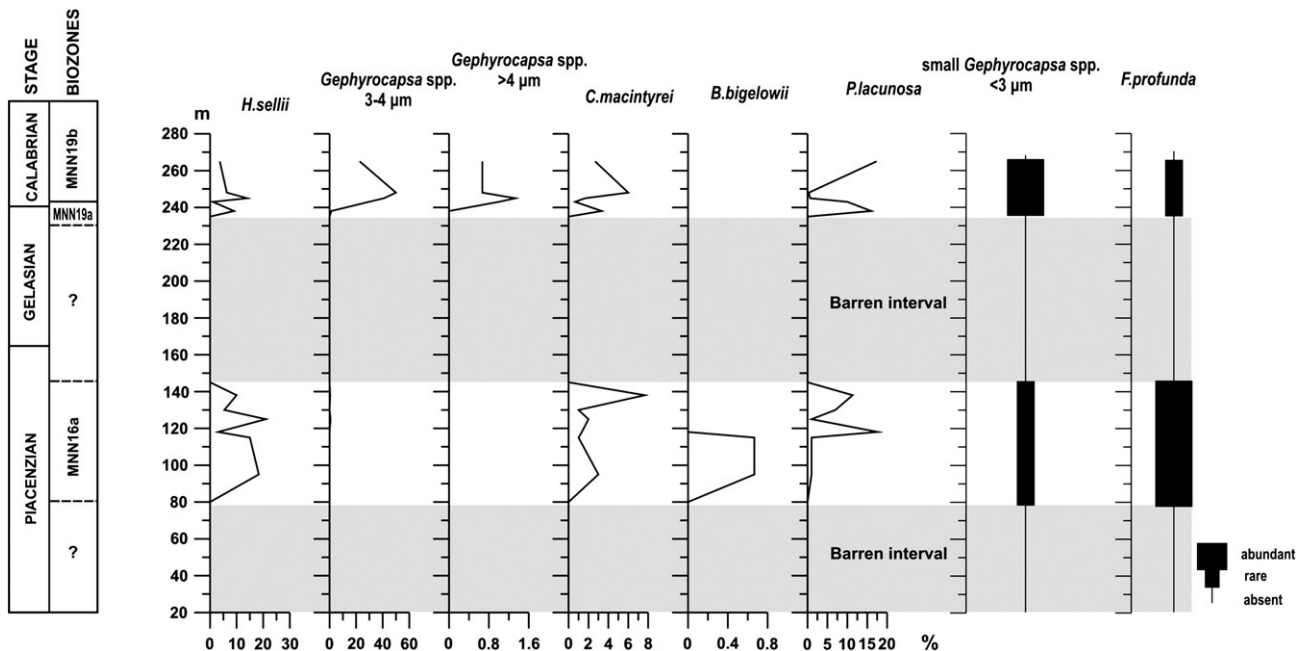


Fig. 12. Relative abundance patterns of calcareous nannofossil species through the upper Pliocene–lower Pleistocene succession of northern Milos. Biozonal scheme is after Rio et al. (1990).

Table 4
Summary of microfossils from the upper Pliocene–lower Pleistocene succession of northern Milos. Data on macrofossils for Diatomite Unit III are from [Sonder \(1924\)](#) and [Fytikas \(1977\)](#).

Lithological units	Calcareous nannofossils	Diatoms	Planktonic–benthic foraminifera	Macrofossils
Diatomite Unit I		<i>Rophadolia</i> , <i>Actinocyclus</i> spp., <i>Rhizosolenia</i> , <i>Grammatophora</i>	Barren	
Diatomite Unit II	<i>Helicosphaera sellii</i> , <i>Calcidiscus macintyreii</i> , <i>Pseudoemiliania lacunosa</i> , <i>Braarudosphaera</i> spp., very rare <i>Discoaster asymmetricus</i> , <i>D. tamalis</i> , <i>D. triradiatus</i> , rare small <i>Gephyrocapsa</i> spp., abundant <i>Florisphaera profunda</i>	<i>Rophadolia</i> , <i>Rhizosolenia</i> , <i>Thalassiosira</i> , <i>Nitzschia</i> , <i>Hemidiscus</i> , <i>Actinocyclus</i>	<i>Globigerina bulloides</i> , <i>G. falconensis</i> , <i>G. quinqueloba</i> , <i>Globigerinoides ruber</i> , <i>G. quinqueloba</i> , <i>Neogloboquadrina pachyderma</i> , <i>Orbulina universa</i> , <i>Cibicides lobatulus</i>	
Diatomite Unit III	<i>Helicosphaera sellii</i> , <i>Calcidiscus macintyreii</i> , <i>Pseudoemiliania lacunosa</i> , <i>Gephyrocapsa</i> spp. >4 µm, abundant small <i>Gephyrocapsa</i> spp.	<i>Stephanopyxix</i> and <i>Amphora</i> forms, <i>Rhizosolenia</i> , <i>Rophadolia</i> , <i>Nitzschia</i> , <i>Hemidiscus</i>	<i>Globigerinoides saculifer</i> , <i>Globigerinella aequilateralis</i> and <i>Globorotalia inflata</i> .	Bivalves (<i>Chlamys</i> spp., <i>Pecten</i> , <i>Isocardia</i> , <i>Solecardia</i> , <i>Pinna</i> , <i>Ostrea</i> , <i>Chama</i> , <i>Lucinopsis</i>), scaphopods (<i>Dentalium</i>), gastropods (<i>Scala</i>), brachiopods (<i>Terebratula</i> spp.), echinoids (<i>Arbacia</i> , <i>Psammechinus</i> , <i>Schizaster</i> , <i>Lytechinus</i> , <i>Brissopsis</i> , <i>Prostagantus</i>)
Diatomite Unit IV		<i>Stephanopyxix</i> and <i>Amphora</i> forms, <i>Rhizosolenia</i> , <i>Rophadolia</i> , <i>Nitzschia</i> , <i>Hemidiscus</i>	<i>Globigerina bulloides</i> , <i>G. quinqueloba</i> , <i>G. falconensis</i> , <i>Globigerinoides ruber</i> , <i>Neogloboquadrina pachyderma</i>	

within the lithic laminae of the diatomaceous marlstone as well as in the terrigenous fraction of the remaining fossiliferous sedimentary lithofacies.

The location of eruption centres changed throughout the late Pliocene–early Pleistocene in northern Milos. Submarine cryptodome– pumice cone volcanoes, e.g. the Filakopi cryptodome located east of the study area, were emplaced at several points where Milos Island is now situated ([Stewart and McPhie, 2006](#)). [Rinaldi and Campos Venuti \(2003\)](#) identified the Bombarda volcano, south of the study area. Other eruption centres, in particular those causing accumula- tion of the lowermost volcaniclastic units, may be located in the islets of Polyegos and Kimolos, a few kilometres north of Milos ([Francalanci et al., 2007](#)), or are currently submarine.

Accommodation space available for both development and distri- bution of the upper Pliocene–lower Pleistocene rocks of northern Milos resulted from the combined effect of submarine volcanism and sea-level changes. Several episodes of sea-level rise and drop can be identified on the basis of local unconformities and/or major truncations throughout the stratigraphic succession. In the following paragraphs, a summary of stratigraphic discontinuities and major depositional changes (named ‘events’ in [Fig. 14](#)) from bottom to top of the sequence is presented.

Deposits from Diatomite Unit I and Volcaniclastic Unit II are bounded by a sharp erosive contact (Event A; [Fig. 14](#)) that resulted from redeposition of clast- to sand-sized pumiceous deposits over a relatively deep-marine diatomaceous marlstone. This event likely

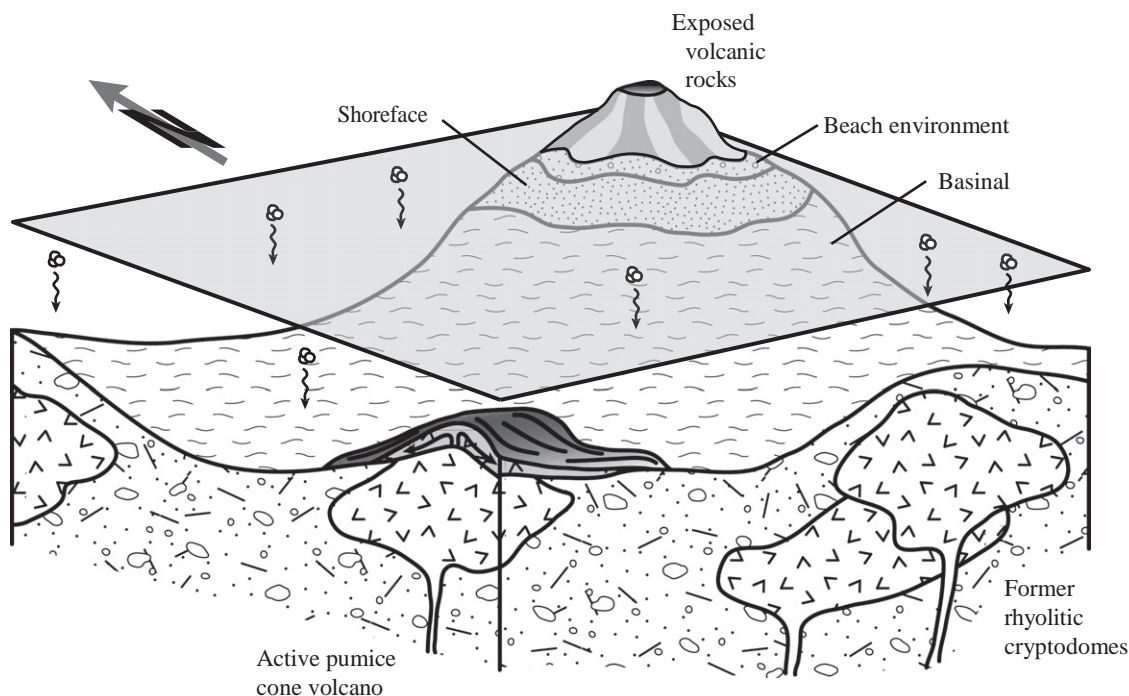


Fig. 13. Palaeoenvironmental reconstruction of depositional settings in Milos Island during the late Pliocene–early Pleistocene. Most of the volcanic activity and associated volcanic products as well as sedimentation processes took place in a marine environment. Locations of main volcanic intrusion centres are approximate. Graphic design is inspired on [Stewart and McPhie \(2006\)](#).

indicates sea-level drop and/or readjustment of the submarine deposits due to volcanic-induced instability. Volcaniclastic Unit I can be tentatively correlated with the Agios Konstatinos Pumice Breccia (see Fig. 2 in Stewart and McPhie, 2004).

After deposition of a thick sequence of alternating laminated diatomaceous marlstone and sandy limestone deposits, the development of cross-stratified, brachiopod-rich (*Terebratula* spp.) sandstone facies (Event B; Fig. 14) points to a stage of remarkable shallowing. This facies is representative of beach deposits directly overlying shoreface and basinal facies characteristic of Diatomite Unit II. An up section change from the foreshore facies to shoreface sandy limestone and further accumulation of coarse pumice breccia of the lower part of Volcaniclastic Unit III indicates rapid sea-level rise. These deposits can be stratigraphically correlated with the Filakopi Pumice Breccia (FPB) of Stewart and McPhie (2004) who provided an upper age limit for the submarine pumice breccias at about 2.66 ± 0.07 Ma, similar to that obtained by SHRIMP U–Pb in zircon dating of the Kalogeros dacitic cryptodome (Stewart and McPhie, 2003a, 2006).

A sharp contact between volcaniclastic and shallow-water fossiliferous deposits at the top of the coarse pumice breccia facies indicates an internal truncation in Volcaniclastic Unit III (Event C; Fig. 14), probably related to large-scale tilting. The fossiliferous deposits above the contact are up to 8 m thick and show rapid lateral thinning into 0.60 m thick beds, and even disappear under a package of volcaniclastic deposits. This feature together with the strong soft-sediment deformation of the fossiliferous sedimentary beds points to readjustment of the geometry of seafloor prior to the emplacement of a felsic cryptodome–pumice cone volcano. According to this stratigraphic scheme, most of Volcaniclastic Unit III can be correlated with the Papafragas Formation (Fytikas, 1977; see Fig. 2 in Stewart and McPhie, 2004).

The onset of shallow marine sedimentation of Diatomite Unit III (Event D; Fig. 14) followed rapid accumulation of the pumiceous deposits of Volcaniclastic Unit III. The contact between the two units is sharp. Deposition of fossiliferous-rich, burrowed sandy limestone above the contact is underlined by the occurrence of aligned volcanic blocks. The Gelasian/Calabrian boundary (1.805 Ma) has been identified within the laminated diatomaceous marlstone deposits of Diatomite Unit III. The dating allows stratigraphic correlation with previously defined stratigraphic formations in other Greek locations where the lower Pleistocene record is exposed (e.g. Papanikolaou et al., 2011). The sedimentary deposits of Diatomite Unit III can be correlated with the Sarakiniko Formation.

The stratified pumice deposits of Volcaniclastic Unit IV unconformably overlie the fossiliferous rocks of Diatomite Unit III (Event E; Fig. 14). The volcaniclastic deposits are interpreted to be related to the submarine eruption of the Bombardo volcano, dated as ~ 1.7 Ma (Rinaldi and Campos Venuti, 2003). An alternative interpretation suggests a genetic relation to the Korakia Andesite, dated at 1.8 Ma (Kondopoulou and Pavlides, 1990) but the predominance of felsic pumice blocks and ash in Volcaniclastic Unit IV better conforms the former interpretation.

Deposition of Diatomite Unit IV represents the last episode of clearly marine sedimentation in northern Milos. Sedimentation over volcanic deposits of Volcaniclastic Unit IV (Event F; Fig. 14) started directly with vaguely laminated marlstone that passes rapidly into laminated diatomaceous marlstone. This suggests relatively deep sea depositional conditions for both the top of the volcaniclastic unit and the diatomaceous deposits. The rest of Diatomite Unit IV reflects changes in water depth trending to progressively shallow water, as indicated by development of burrowed sandy limestone at the top of the unit. The transition from the fossiliferous marine deposits to Volcaniclastic Unit V, which shows reworking by shallow-water currents, is mainly covered, thus prohibiting clear interpretation of the evolution of the depositional setting.

7. Conclusions

The upper Pliocene–lower Pleistocene succession of northern Milos records an alternation of explosive volcanic products and fossiliferous sedimentary rocks. Four main sedimentary facies representative of varied submarine depositional environments are recognised: i) laminated diatomaceous marlstone, ii) massive sandy limestone, iii) cross-stratified, brachiopod-rich (*Terebratula* spp.) sandstone, and iv) wave-rippled sandstone and siltstone.

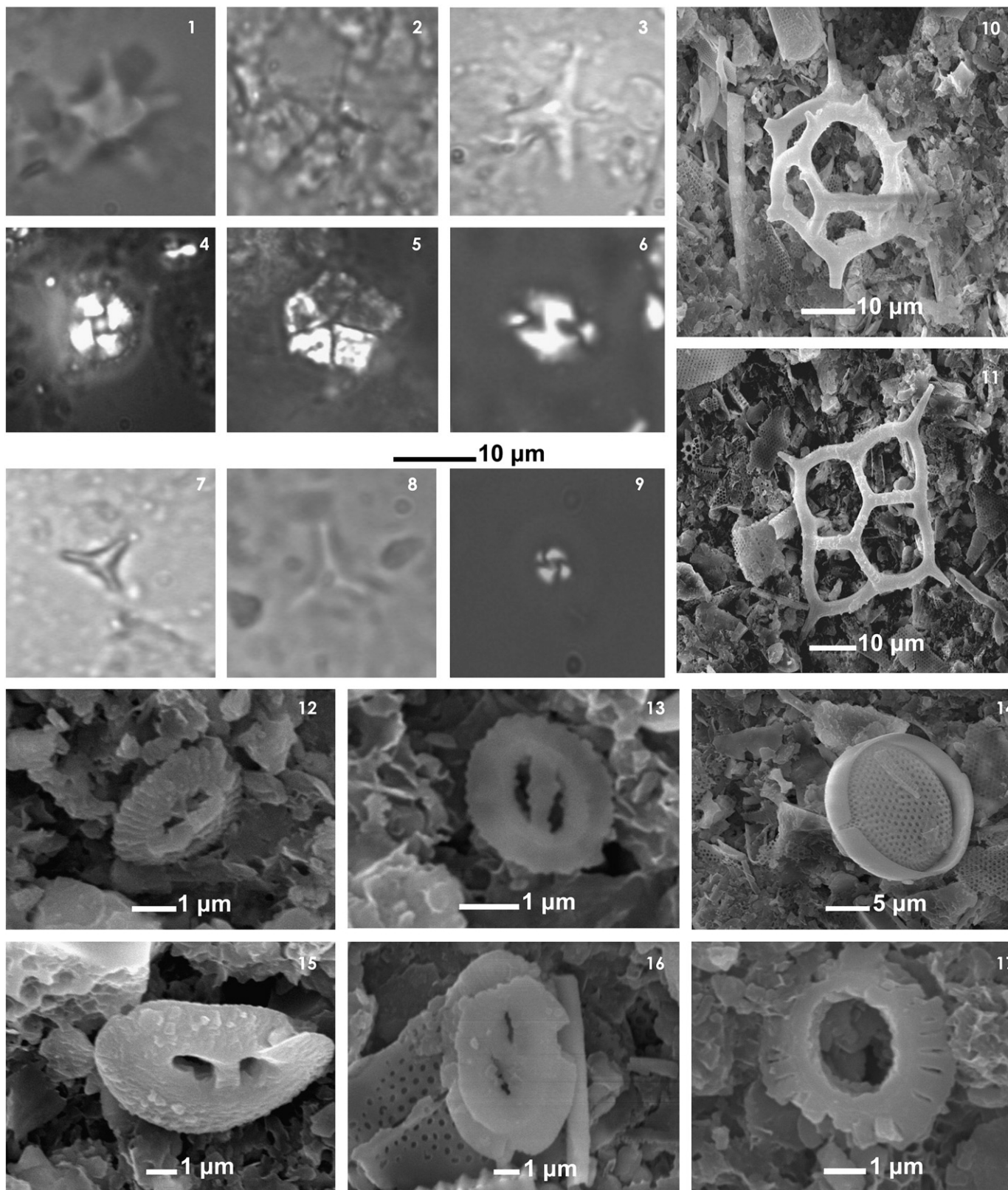
Laminated diatomaceous marlstone is the most common sedimentary deposit and consists of lithic and biogenic couplets where reworked volcanic grains are associated with dense accumulations of diatoms, calcareous nannofossils, and foraminifera. Deposition of diatomaceous marlstone took place in a number of silled, relatively shallow basins where water stratification and oxygen-deficient conditions prevailed. The presence of local burrows (*Ophiomorpha*?) at several intervals of the laminated diatomaceous deposits points to episodes of improved benthic oxygenation. Cyclic facies association of the diatomaceous marlstone with burrowed sandy limestone indicates oscillations in water depth that may have resulted from sea-level changes and/or emplacement of submarine volcanic cones.

Volcanic activity during the development of the upper Pliocene–lower Pleistocene succession was closely related to the emplacement of cryptodome–pumice cone volcanoes. Rhyolitic intrusion centres produced vast accumulations of coarse pumice breccia and associated finer-grained pumiceous deposits that underwent extensive reworking by shallow-marine and turbidite flows.

Six major events reflecting episodes of volcanic emplacement, changes in sea-floor morphology and sea-level changes are recorded throughout the succession. On the basis of calcareous nannofossils, the Gelasian/Calabrian boundary (formerly Pliocene–Pleistocene boundary) is identified within Diatomite Unit III. The dating is consistent with existing radiometric data and allows stratigraphic correlation with previously defined stratigraphic formations in Milos Island and other Greek locations where the lower Pleistocene stratigraphic record is exposed.

Acknowledgements

Special thanks are owed to the following colleagues who provided both scientific and technical assistance. Juan Usera (University of Valencia) is thanked for his help in determination of planktonic foraminifera. María José López-García (National Museum of Natural Sciences, Madrid) provided scientific guidance on the study of diatom assemblages. Adriana Bellanca and Rodolfo Neri (University of Palermo) participated in profitable scientific discussion and helped with petrographical and geochemical studies. Ulrich Lutat (Silver & Baryte Co) provided field assistance. Thanks are given to Dimitris Fragoulis, from TITAN Co for his kindness in providing XRF analyses. Manuel Pozo (University Autónoma of Madrid) is thanked for helping in XRD determinations. Jesús Caracuel (University of Alicante), who has unfortunately since passed away, helped in ichnological analysis. María José Huertas is especially thanked for her comments on volcanological processes and products. We are also indebted to Thomas Stevens (Royal Holloway, London) who helped in refining the final version of the paper. Technical and scientific assistance by Pedro Castiñeiras is greatly appreciated. Two anonymous reviewers and the Editor-in-Chief Finn Surlyk are thanked for their constructive and valuable reviews that considerably improved an earlier version of the manuscript. The work has been supported by Projects PB97-0244 and CGL2008-05813-C02-02 (Spanish Ministry of Science and Innovation), by the Greek General Secretariat of Research & Technology (GSRT), and it has benefited from Greek–Spanish bilateral cooperation programmes. For financial support we are also indebted to the University Complutense of Madrid (Research Group BSCH UCM-910607).



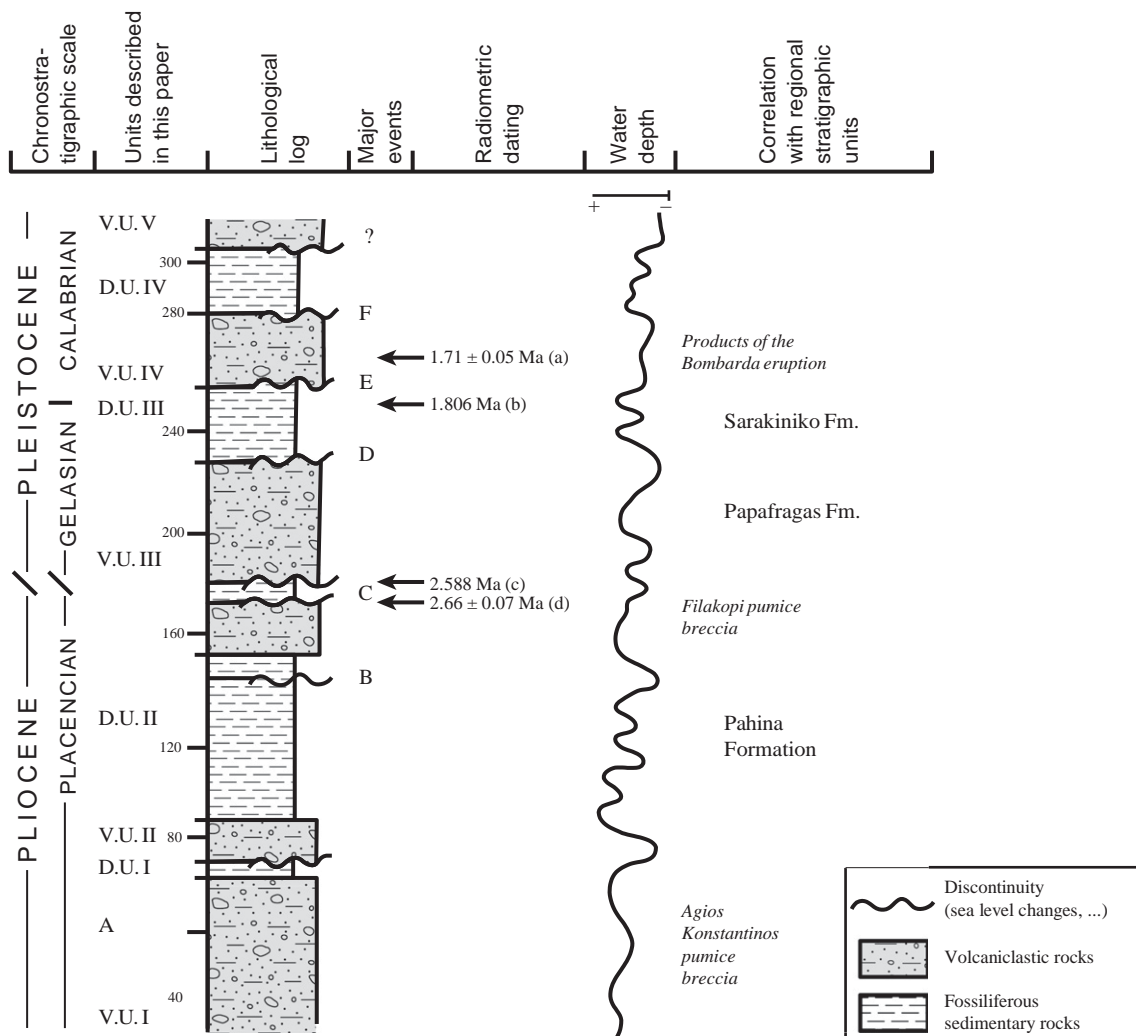


Fig. 14. Summary of major geological events recorded in the upper Pliocene–lower Pleistocene succession of northern Milos. References for radiometric dating are as follows: (a) Rinaldi and Campos Venuti (2003); based on Fytikas et al. (1986); (b) Gelasian/Calabrian boundary; Gibbard et al. (2009); (c) Stewart and McPhie (2006); (d) Pliocene/ Pleistocene boundary; Gibbard et al. (2009).

References

- Angelier, J., Lyberis, N., Le Pichon, X., Barrier, E., Huchon, P., 1982. The tectonic development of the Hellenic Arc and the Sea of Crete: a synthesis. *Tectonophysics* 86, 159–196.
- Bellas, S., Frydas, D., 1994. Calcareous and siliceous phytoplankton stratigraphy from Neogene deposits of Milos Island (Cyclades, Greece). *Bulletin of the Geological Society of Greece* 30, 363–372.
- Castradori, D., 1993. Calcareous nannofossils and the origin of Eastern Mediterranean sapropels. *Paleoceanography* 8, 459–471.
- Collinson, J., 1994. Sedimentary deformational structures. In: Maltman, A. (Ed.), *The Geological Deformation of Sediments*. Chapman & Hall, London, pp. 95–125.
- Francalanci, L., Vougioukalakis, G.E., Fytikas, M., 2007. Petrology and volcanology of Kimolos and Polyegos volcanoes within the context of the South Aegean Arc, Greece. In: Beccaluva, L., Bianchini, G., Wilson, M. (Eds.), *Cenozoic volcanism in the Mediterranean area: Geol. Soc. America Spec. Paper*, 418, pp. 33–65.
- Frydas, D., 1992. Silicoflagellés et Diatomées du Pleistocène inférieur de l'île de Milos: coupe d'Adamas SE (Cyclades, Grèce). *Géologie Méditerranéenne* 19, 231–247.
- Frydas, D., 1996a. Silicoflagellate stratigraphy for Neogene to Quaternary marine sediments in Greece. *Newsletters on Stratigraphy* 32, 99–116.
- Frydas, D., 1996b. Upper Zanclean silicoflagellates from Milos Island (Cyclades, Greece). *Journal of Nannoplankton Research* 18, 61–67.
- Fytikas, M., 1977. Geological Map of Milos 1:25 000. Institute of Geology and Mineral Exploration (IGME), Athens, Greece.
- Fytikas, M., Vougioukalakis, G., 1995. Pre-meeting Field-trip to Milos. I.G.C.P. Project 356, 3rd Annual Meeting, IUGS-UNESCO, Guidebook.
- Fytikas, M., Vougioukalakis, G. (Eds.), 2005. *The South Aegean Active Volcanic arc. Present knowledge and future perspectives. : Developments in Volcanology*, 7. Elsevier Publ. Co., Amsterdam.
- Fytikas, M., Giuliani, O., Innocenti, F., Marinelli, G., Mazzuoli, R., 1976. Geochronological data on recent magmatism of the Aegean Sea. *Tectonophysics* 31, T29–T34.

Plate I. Calcareous nannofossil, silicoflagellate and diatom specimens from Diatomite Units II and III. Images from light microscope (LM) and scanning electron microscope (SEM) Jeol JSM 6360 (Dept. of Hist. Geology-Paleontology, University of Athens). 1–2. *Discoaster asymmetricus* calcareous nannofossil/nannolith (LM) in moderate state of preservation, very rare specimens most probably due to the eutrophic environment of the diatomaceous deposits, sample ALM 9; 3. *Discoaster tamalis* calcareous nannofossil/nannolith (LM), nannofossil zone MNN16a, sample ALM 9; 4. *Calcidiscus macintyreii* calcareous nannofossil/placolith (LM), sample ALM 9; 5. *Braarudosphaera bigelowii* calcareous nannofossil (LM) characteristic of fresh-water input, sample ALM 13; 6. *Helicosphaera sellii* calcareous nannofossil/helicolith (LM), sample ALM 9; 7–8. *Discoaster triradiatus* calcareous nannofossil/nannolith (LM), sample ALM 13; 9. *Gephyrocapsa* spp. > 4 µm, calcareous nannofossil/placolith (LM), featuring nannofossil biozone MNN19a, sample ALM 23; 10. Well preserved silicoflagellate *Distephanus* sp. (SEM), sample ALM 9, (in the same image, well preserved but broken sponge spicule (left) and highly altered diatom frustules due to transport and redeposition); 11. Well preserved silicoflagellate *Dictyocha* sp. (SEM) resting on highly altered diatom frustules, sample ALM 9; 12. *Gephyrocapsa* spp. > 4 µm, calcareous nannofossil/placolith (SEM), sample ALM 23; 13. Small *Gephyrocapsa* spp., calcareous nannofossil/placolith (SEM), sample ALM 13; 14. Well preserved centric diatom *Cyclotella* sp. (SEM), resting on highly altered diatom frustules (the coexistence probably indicates a coeval clastic and pelagic deposition of the diatom frustules) sample ALM 9; 15. *Helicosphaera sellii* calcareous nannofossil/helicolith from the distal side (SEM), sample ALM 13; 16. *Helicosphaera sellii* nannofossil/helicolith from the proximal side (SEM), sample ALM 9; 17. *Pseudoe-miliania lacunose* calcareous nannofossil/placolith (SEM), sample ALM 13.

- Fytikas, M., Innocenti, F., Kolios, N., Manetti, P., Mazzuoli, R., Poli, G., Rita, F., Villari, L., 1986. Volcanology and petrology of volcanic products from the island of Milos and the neighbouring islets. *Journal of Volcanology and Geothermal Research* 28, 297–317.
- Gibbard, P.L., Head, M.J., Walker, M.J.C., The Subcommission on Quaternary Stratigraphy, 2009. Formal ratification of the Quaternary System/Period and the Pleistocene Series/Epoch with a base at 2.58 Ma. *Journal of Quaternary Science*. doi:10.1002/jqs.1338.
- Jackson, J.A., 1994. Active tectonics of the Aegean region. *Annual Review of Earth and Planetary Sciences* 22, 239–271.
- Jones, A.P., Omoto, K., 2000. Towards establishing criteria for identifying trigger mechanisms for soft-sediment deformation: a case study of Late Pleistocene lacustrine sands and clays, Onikobe and Nakayamadaira Basins, northeastern Japan. *Sedimentology* 47, 1211–1226.
- Kondopoulou, D.P., Pavlides, S.B., 1990. Paleomagnetic and neotectonic evidence for different deformation patterns in the south Aegean Volcanic Arc: the case of Milos Island. *Proceedings of the International Earth Science Congress on Aegean Regions*, Izmir, pp. 210–233.
- Le Pichon, X., Angelier, J., 1979. The Aegean Sea. *Philosophical Transactions of the Royal Society of London Series A* 300, 357–372.
- Lourens, L., Hilgen, F., Shackelton, N.J., Laskar, J., Wilson, D., 2004. The Neogene Period. In: Gradstein, F.M., Ogg, J.G., Smith, A.G. (Eds.), *A Geological Time Scale*. Cambridge Univ. Press, Cambridge, pp. 409–440.
- McKenzie, D.P., 1978. Active tectonics of the Alpine Himalayan belt: the Aegean Sea and surrounding areas. *Geophysical Journal of the Royal Astronomical Society* 55, 217–254.
- Meulenkamp, J.E., Wortel, M.J.R., Van Wamel, A.A., Spakman, W., Hoogerduyn Strating, E., 1988. On the Hellenic subduction zone and the geodynamic evolution of Crete since the late Middle Miocene. *Tectonophysics* 146, 203–215.
- Molfinio, B., McIntyre, A., 1990. Precessional forcing of nutricline dynamics in the Equatorial Atlantic. *Science* 249, 766–769.
- Negri, A., Giunta, S., 2001. Calcareous nannofossil paleoecology in the sapropel S1 of the Eastern Ionian Sea: paleoceanographic implications. *Palaeogeography, Palaeoclimatology, Palaeoecology* 169, 101–112.
- Okada, H., Honjo, S., 1973. The distribution of ocean coccolithophorids in the Pacific. *Deep Sea Research* 20, 355–374.
- Owen, G., 1996. Experimental soft-sediment deformation: structures formed by the liquefaction of unconsolidated sands and some ancient examples. *Sedimentology* 43, 279–293.
- Papanikolaou, M., Triantaphyllou, M., Platzman, E., Gibbard, P., Macniocail, C., Head, M.J., 2011. A well established Early–Middle Pleistocene marine sequence on SE Zakynthos island, Western Greece: magneto-biostratigraphic constraints and palaeoclimatic implications. *Journal of Quaternary Science* 26, 523–540.
- Pe-Piper, G., Piper, D.J.W., 1989. Spatial and temporal variation in Late Cenozoic back-arc volcanic rocks, Aegean Sea region. *Tectonophysics* 169, 113–134.
- Pe-Piper, G., Piper, D.J.W., 2005. The South Aegean active volcanic arc: relationships between magmatism and tectonics. In: Fytikas, M., Voulgoulakakis, G. (Eds.), *The South Aegean Active Volcanic arc. Present knowledge and future perspectives*. : Developments in Volcanology, 7. Elsevier Publ. Co., Amsterdam.
- Perch-Nielsen, K., 1985. Cenozoic calcareous nannofossils. In: Bolli, H.M., Saunders, J.B., Pech-Nielsen, K. (Eds.), *Plankton Stratigraphy*. Cambridge Univ. Press, Cambridge, pp. 427–554.
- Raffi, I., Backman, J., Fornaciari, E., Palike, H., Rio, D., Lourens, L., Hilgen, F., 2006. A review of calcareous nannofossil astrochronology encompassing the past 25 million years. *Quaternary Science Reviews* 25, 3113–3137.
- Rinaldi, M., Campos Venuti, M., 2003. The submarine eruption of the Bombarda volcano, Milos Island, Cyclades, Greece. *Bulletin of Volcanology* 65, 282–293.
- Rio, D., Fornaciari, E., Raffi, I., 1990. Late Quaternary through early Pleistocene calcareous nannofossils from the western equatorial Indian Ocean (Leg 115). *ODP Proceed. Sci. Results*, pp. 175–235.
- Royden, L.H., Papanikolaou, D.J., 2011. Slab segmentation and late Cenozoic disruption of the Hellenic arc. *Geochemistry, Geophysics, Geosystems* 12. doi:10.1029/2010GC003280.
- Sancetta, C., 1996. Laminated diatomaceous sediments: controls on formation and strategies for analysis. In: Kemp, A.E.S. (Ed.), *Palaeoclimatology and palaeoceanography from laminated sediments*. Geol. Soc. Spec. Publ., 116, pp. 17–21.
- Schminke, H.U., 2004. *Volcanism*. Springer, Berlin. 324 pp.
- Sonder, R.A., 1924. Zur geologie und petrographie der inselgruppe con Milos. *Zeitschrift für Vulkanologie* 8, 181–237.
- Stamatakis, M.G., 2003. Characterization of biogenic amorphous silica deposits in Greece and their industrial potential. In: Eliopoulos, D.G., et al. (Ed.), *Mineral Exploration and Sustainable Development*, 2. Millpress, Rotterdam, pp. 927–930.
- Stamatakis, M.G., Lutat, U., Regueiro, M., Calvo, J.P., 1996. Milos. The mineral island. *Industrial Minerals*, pp. 57–61. February 1996, London.
- Stamatakis, M.G., Fragoulis, D., Antonopoulou, S., Stamatakis, G., 2010. The opaline silica-rich sedimentary rocks of Milos Island, Greece, and their behaviour as pozzolans in the manufacture of cement. *Advances in Cement Research* 22, 171–183.
- Stewart, A.L., McPhie, J., 2003a. Internal structure and emplacement of an Upper Pliocene dacite cryptodome, Milos Island, Greece. *Journal of Volcanology and Geothermal Research* 124, 129–148.
- Stewart, A.L., McPhie, J., 2003b. Facies architecture of the submarine-to-subaerial volcanic succession on Milos, Greece. *International Conference on the South Aegean Active Volcanic Arc: Present Knowledge and Future Perspectives (SAAVA 2003)*, Book of Abstracts, 24.
- Stewart, A.L., McPhie, J., 2004. An Upper Pliocene coarse pumice breccia generated by a shallow submarine explosive eruption, Milos, Greece. *Bulletin of Volcanology* 66, 15–28.
- Stewart, A.L., McPhie, J., 2006. Facies architecture and Late Pliocene–Pleistocene evolution of a felsic volcanic island, Milos, Greece. *Bulletin of Volcanology* 68, 703–726.
- Traineau, H., Dalabakis, P., 1989. Mise en évidence d'une éruption phréatique historique sur l'île de Milos (Grèce). *Comptes Rendus de l'Académie des Sciences Paris* 308, 247–252.
- Triantaphyllou, M.V., Antonarakou, A., Kouli, K., Dimiza, M., Kontakiotis, G., Papanikolaou, M., Ziveri, P., Mortyn, P.G., Lianou, V., Lykousis, V., Dermitzakis, M.D., 2009a. Late Glacial–Holocene ecostratigraphy of the south-eastern Aegean Sea, based on plankton and pollen assemblages. *Geo-Marine Letters* 29, 249–267.
- Triantaphyllou, M., Ziveri, P., Gogou, A., Marino, G., Lykousis, V., Bouloubassi, I., Emeis, K.C., Kouli, K., Dimiza, M., Rosell-Mele, A., Papanikolaou, M., Katsouras, G., Nunez, N., 2009b. Late Glacial–Holocene climatic variability at the southeastern margin of the Aegean Sea. *Marine Geology* 266, 182–197.
- Triantaphyllou, M.V., Antonarakou, A., Dimiza, M., Anagnostou, Ch., 2010. Calcareous nannofossils and planktonic foraminiferal distributional patterns during deposition of sapropels S6, S5 and S1 in the Lybian Sea (Eastern Mediterranean). *Geo-Marine Letters* 30, 1–13.
- Tucker, M.E., 2001. *Sedimentary Petrology*, 3rd ed. Blackwell Science, Oxford. 262 pp.
- van Hinsbergen, D.J.J., Snel, E., Garstman, S.A., Marunteanu, M., Langereis, C.G., Wortel, M.J.R., Meulenkamp, J.E., 2004. Vertical motions in the Aegean volcanic arc: evidence for rapid subsidence preceding in situ volcanism. *Marine Geology* 209, 329–345.
- Vincent, P., 2000. Volcanoes: from magmas to tephra and epivolcaniclastics. In: Leyrit, H., Montanet, Ch. (Eds.), *Volcaniclastic Rocks, from Magmas to Sediments*. Gordon and Breach Science Publishers, pp. 1–32.
- Zeilinga de Boer, J., 1989. The Greek enigma: is development of the Aegean orogene dominated by forces related to subduction or obduction? In: Makris, J. (Ed.), *Geological Aspects and Tectonic Evolution of Mediterranean Seas*. Mar. Geol., 87, pp. 31–54.